Hard wall - soft wall - vorticity scattering in shear flow

EINDHOVEN UNIVERSITY OF TECHNOLOGY
Department of Mathematics and Computer Science

CASA-Report 14-17
May 2014

Hard wall – soft wall – vorticity scattering in shear slow

by

S.W. Rienstra, D.K. Singh

Centre for Analysis, Scientific computing and Applications
Department of Mathematics and Computer Science
Eindhoven University of Technology
P.O. Box 513
5600 MB Eindhoven, The Netherlands
ISSN: 0926-4507

Hard wall – soft wall – vorticity scattering in shear flow

Sjoerd W. Rienstra* and Deepesh Kumar Singh†

Department of Mathematics and Computer Science, TU Eindhoven, The Netherlands

An analytically exact solution, for the problem of low Mach number incident vorticity scattering at a hard-soft wall transition, is obtained in the form of Fourier integrals by using the Wiener-Hopf method. Harmonic vortical perturbations of inviscid linear shear flow are scattered at the wall transition. This results in a far field which is qualitatively different for low shear and high shear cases. In particular, for high shear the pressure (apparently driven by the mean flow) does not decay and its Fourier representation involves a diverging integral which is to be interpreted in generalised sense.

Then the incompressible hydrodynamic (Wiener-Hopf) "inner" solution is matched asymptotically to an acoustic outer field in order to determine the sound associated to the scattering. The qualitative difference between low and high shear is also apparent here. The low shear case matches successfully. In the high shear case only a partial matching was possible.

I. Introduction

The effect of boundaries, in particular soft or flexible boundaries, on the aerodynamic noise generated by turbulent flows in general and vortical perturbations in particular have been studied for decades. (See for example [1,2,3,4,5,6], which is just a minute fraction of the literature.) If the Mach number of the flow is small, the spectral component of the boundary layer pressure perturbations, *i.e.* the Fourier transform of pressure in the plane of boundary layer, have subsonic phase velocities which constitute a strong local field but decays exponentially with distance from the flow. If there is a discontinuity in the boundary, the flow may use it as a "wave number converter" to scatter far field noise [7]. So the main sound production concentrates at discontinuities. This was confirmed by Crighton [2] who studied in detail the radiation from the flow over 2 semi-infinite planes that differ in their inertia and elastic properties. There is, however, a need for canonical model problems that allows analytically exact solutions of vorticity in shear flow scattering at hard-soft transitions of a liner wall which is demonstrated in the current work.

In the current paper, the scattering of 2D vorticity perturbations in an inviscid low Mach number shear flow (with vanishing velocity at the wall) passing over a hard to soft transition of this wall has been examined.

*Associate Professor, Dept. Math. & Comp. Sc., Eindhoven Univ. of Techn., Netherlands, Senior Member AIAA.

†Doctoral candidate, Dept. Mathematics & Computer Science, Eindhoven University of Technology, Netherlands.

The incident field is assumed to be produced by a mass source far upstream, although a non-conservative force field would give similar results. Following [8], a 2D vorticity χ with mass source Q, satisfying

$$\rho\Big(\frac{\partial}{\partial t}+\boldsymbol{v}\cdot\nabla\Big)\Big(\frac{\chi}{\rho}\Big)=-\frac{\chi}{\rho}Q. \tag{1}$$

is considered. If the source is small, located in a bounded region $\mathcal{G}$, and induces harmonic isentropic perturbations to a parallel sheared flow U with otherwise constant density ρ_0 and sound speed c_0 given by

$$\boldsymbol{v}=U(y)\boldsymbol{e}_x+\hat{\boldsymbol{v}}\,\mathrm{e}^{\mathrm{i}\omega t},\quad \chi=-U'(y)+\hat{\chi}\,\mathrm{e}^{\mathrm{i}\omega t},\quad \rho=\rho_0+c_0^{-2}\hat{p}\,\mathrm{e}^{\mathrm{i}\omega t},\quad Q=\hat{q}\,\mathrm{e}^{\mathrm{i}\omega t}, \tag{2}$$

then we have after linearisation and writing $U(y_0)=U_0$, $U'(y_0)=\sigma_0$,

$$\rho_0\Big(\mathrm{i}\omega+U(y)\frac{\partial}{\partial x}\Big)\Big(\hat{\chi}+\frac{U'(y)}{\rho_0c_0^2}\hat{p}\Big)=U'(y)\hat{q}=\iint_{\mathcal{G}}\big[\sigma_0\hat{q}(x_0,y_0)\delta(x-x_0)\delta(y-y_0)\big]\mathrm{d}x_0\mathrm{d}y_0. \tag{3}$$

This has, under causal free field conditions (allowing only perturbations generated by the source) and $U_0>0$, the solution [8]

$$\hat{\chi}+\frac{U'(y)}{\rho_0c_0^2}\hat{p}=\iint_{\mathcal{G}}\left[\frac{\hat{q}(x_0,y_0)\sigma_0}{\rho_0U_0}H(x-x_0)\,\mathrm{e}^{-\mathrm{i}k_0(x-x_0)}\,\delta(y-y_0)\right]\mathrm{d}x_0\mathrm{d}y_0,\quad k_0=\frac{\omega}{U_0}. \tag{4}$$

Downstream the source we have just $H(x-x_0)=1$. Utilising linearity we will consider a single (x_0,y_0)-component with unit amplitude and phase factor $\mathrm{e}^{\mathrm{i}k_0x_0}=1$, in the incompressible limit, leading to the vortex sheet

$$\hat{\chi}=\frac{\sigma_0}{\rho_0U_0}\,\mathrm{e}^{-\mathrm{i}k_0x}\,\delta(y-y_0). \tag{5}$$

With a simple shear flow given by $U(y)=\sigma y$ and uniform boundary conditions along the wall $y=0$, the corresponding velocity and pressure fields can be determined, far enough downstream the source, relatively easily. This field will act as the incident field for our scattering problem.

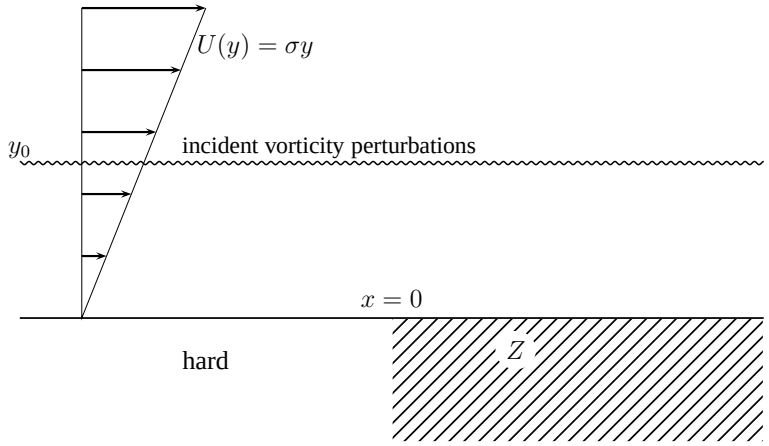

Figure 1. Sketch of the problem

II. Model

We summarise the above introduction as follows. Consider the two-dimensional incompressible inviscid problem of perturbations of a linearly sheared mean flow with time dependent ($\mathrm{e}^{\mathrm{i}\omega t}$) vortex sheet along $y = y_0$ in $y > 0$ and a wall at $y = 0$ which is hard for $x < 0$ and soft (impedance) for $x > 0$ with $U(y) = \sigma y$; see figure 1. In this configuration we will have no contribution of a critical layer h_c or an instability like in [9].

As described above, we have a mass source placed at $x = x_0 \to -\infty$, $y = y_0$ which produce the downstream travelling vorticity that decays exponentially away from the line $y = y_0$ in the order $\sim \mathrm{e}^{-k_0|y-y_0|-\mathrm{i}k_0 x}$. When the convected vorticity field hits the hard-to-soft wall transition point $x = 0$, it is scattered into a local pressure field that will radiate as sound into the far field.

The flow in the domain shown in figure 1 is governed by the linearised Euler equations with mixed boundary conditions (hard for $x < 0$ and of impedance type for $x > 0$), which makes the Wiener-Hopf technique [10, 4] a natural choice for obtaining the solution. Once we obtained this (in the context of the acoustic field) inner solution, we can determine the source strength at the singularity $x = 0$. In order to assess the produced sound, the incompressible inner solution will be matched with a compressible (acoustic) outer solution.

III. Mathematical formulation

The governing equation of mass and momentum conservation written in frequency domain are

$$\begin{aligned} \rho_0 \left(\frac{\partial u}{\partial x} + \frac{\partial v}{\partial y} \right) &= 0, \\ \rho_0 \left(\mathrm{i}\omega + U \frac{\partial}{\partial x} \right) u + \rho_0 \frac{\mathrm{d}U}{\mathrm{d}y} v + \frac{\partial p}{\partial x} &= 0, \\ \rho_0 \left(\mathrm{i}\omega + U \frac{\partial}{\partial x} \right) v + \frac{\partial p}{\partial y} &= 0. \end{aligned} \tag{6}$$

Boundary conditions at $y = 0$ are

$$v = 0 \quad \text{if } x < 0,$$

an edge condition of vanishing energy flux from $(0, 0)$, and a wall of impedance $Z = \rho_0 \zeta$ with

$$p = -Zv \quad \text{or} \quad \mathrm{i}\omega p = \zeta p_y \quad \text{if } x > 0.$$

The far field boundary conditions will be of vanishing velocity, but maybe not of vanishing pressure. The incident field (of the undulating vortex sheet at $y = y_0 = U_0/\sigma$) is given by

$$\begin{aligned} u_{\text{in}} &= U_0 \,\mathrm{e}^{-\mathrm{i}k_0 x} \left[-\operatorname{sign}(y - y_0)\ \mathrm{e}^{-k_0|y-y_0|} + \mathrm{e}^{-k_0(y+y_0)} \right], \\ v_{\text{in}} &= \mathrm{i}U_0 \,\mathrm{e}^{-\mathrm{i}k_0 x} \left[\mathrm{e}^{-k_0|y-y_0|} - \mathrm{e}^{-k_0(y+y_0)} \right], \\ p_{\text{in}} &= \frac{\sigma}{\omega} \rho_0 U_0^2 \,\mathrm{e}^{-\mathrm{i}k_0 x} \left[(1 + k_0|y - y_0|)\,\mathrm{e}^{-k_0|y-y_0|} - (1 + k_0(y - y_0))\,\mathrm{e}^{-k_0(y+y_0)} \right], \end{aligned} \tag{7}$$

with $k_0 = \omega/U_0$, and so $k_0 y_0 = \omega/\sigma$. Figure 2 shows pressure and velocities of a typical case.

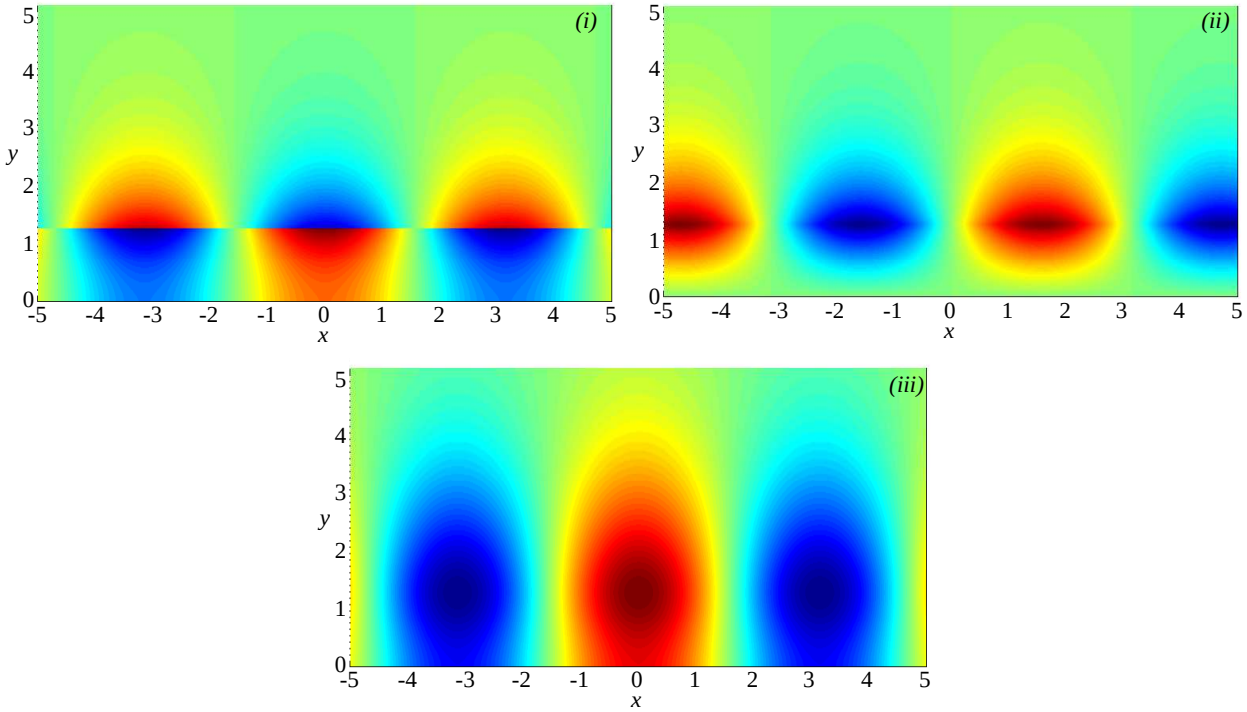

Figure 2. The initial field u_{in}, v_{in} and p_{in} respectively. $\omega = 5, \sigma = 4, U_0 = 5, k_0 = 1, y_0 = 1.25$.

The triple $(u_{\text{in}}, v_{\text{in}}, p_{\text{in}})$ satisfies the differential equation, continuity of p_{in} and v_{in} across $y = y_0$, and the hard-wall boundary condition $v_{\text{in}} = 0$ at $y = 0$. The scattered perturbations are due to the non-vanishing $p_{\text{in}} + Zv_{\text{in}}$ along $y = 0, x > 0$.

We split up the field in the incident part and the scattered part as follows

$$u = u_{\text{in}} + \overline{u}, \quad v = v_{\text{in}} + \overline{v}, \quad p = p_{\text{in}} + \overline{p}. \tag{8}$$

After Fourier transformation in x (formally assuming the convergence of the integrals)

$$\overline{p}(x, y) = \frac{1}{2\pi} \int_{-\infty}^{\infty} \tilde{p}(y, k)\, \mathrm{e}^{-\mathrm{i}kx}\, \mathrm{d}k, \tag{9}$$

(the same for $\overline{u}$ and $\overline{v}$) we obtain the following set of equations

$$\rho_0(-\mathrm{i}k\tilde{u} + \tilde{v}') = 0, \qquad \mathrm{i}\rho_0\Omega\tilde{u} + \rho_0\sigma\tilde{v} - \mathrm{i}k\tilde{p} = 0, \qquad \mathrm{i}\rho_0\Omega\tilde{v} + \tilde{p}' = 0, \tag{10}$$

where $\Omega = \omega - kU$. The system of equations has two independent solutions, namely $\sim \mathrm{e}^{\pm ky}$ [11, 12]. The one, bounded for $y \to \infty$, is then

$$\begin{aligned} \tilde{u}(y) &= kA(k)\, \mathrm{e}^{-|k|y}, \\ \tilde{v}(y) &= -\mathrm{i}|k|A(k)\, \mathrm{e}^{-|k|y}, \\ \tilde{p}(y) &= \rho_0(\Omega - \operatorname{sign}(\operatorname{Re} k)\sigma)A(k)\, \mathrm{e}^{-|k|y}, \end{aligned} \tag{11}$$

with $A(k)$ is to be determined, and

$$|k| = \operatorname{sign}(\operatorname{Re} k)k = \sqrt{k^2}, \tag{12}$$

where $\sqrt{}$ denotes the principal value square root, and $|k|$ has thus branch cuts along the imaginary axis given by $(-\mathrm{i}\infty, 0)$ and $(0, \mathrm{i}\infty)$.

IV. Wiener-Hopf procedure

To facilitate the following Wiener-Hopf procedure, we introduce a small positive parameter ε and have an upper and a lower half plane, and a strip of overlap

$$\mathbb{C}^+ = \{k \in \mathbb{C} \mid \operatorname{Im} k > -\varepsilon\}, \quad \mathbb{C}^- = \{k \in \mathbb{C} \mid \operatorname{Im} k < \varepsilon\}, \quad S = \{k \in \mathbb{C} \mid -\varepsilon < \operatorname{Im} k < \varepsilon\},$$

The physical problem will be the limit $\varepsilon \to 0$ of a regularised problem with k_0 replaced by $k_0 - \mathrm{i}\varepsilon$ (an incident field $\sim \mathrm{e}^{-\mathrm{i}k_0 x}$ slightly decaying with x) and $|k|$ replaced by the smoother function

$$|k| = \sqrt{k^2 + \varepsilon^2}$$

with branch cuts $(-\mathrm{i}\infty, -\mathrm{i}\varepsilon) \cup (\mathrm{i}\varepsilon, \mathrm{i}\infty)$ avoiding strip S (*cf.* [13]).

Introduce the auxiliary functions

$$F_-(k) = \int_{-\infty}^{0} \left[\overline{p}(x,0) + Z\overline{v}(x,0)\right] \mathrm{e}^{\mathrm{i}kx} \,\mathrm{d}x, \quad G_+(k) = \int_0^{\infty} \overline{v}(x,0)\, \mathrm{e}^{\mathrm{i}kx} \,\mathrm{d}x \tag{13}$$

which are analytic in $\operatorname{Im}(k) < 0$ and $\operatorname{Im}(k) > 0$ respectively, and assumed to be analytic in $\mathbb{C}^+$ and $\mathbb{C}^-$. Then we have for G_+

$$G_+(k) = \int_0^{\infty} \overline{v}(x,0)\, \mathrm{e}^{\mathrm{i}kx} \,\mathrm{d}x = \int_{-\infty}^{\infty} \overline{v}(x,0)\, \mathrm{e}^{\mathrm{i}kx} \,\mathrm{d}x = -\mathrm{i}|k|A(k). \tag{14}$$

Furthermore, we have for F_-

$$\begin{aligned} F_-(k) &= \int_{-\infty}^{0} \left[\overline{p}(x,0) + Z\overline{v}(x,0)\right] \mathrm{e}^{\mathrm{i}kx} \,\mathrm{d}x = \int_{-\infty}^{\infty} \left[\overline{p}(x,0) + Z\overline{v}(x,0)\right] \mathrm{e}^{\mathrm{i}kx} \,\mathrm{d}x + \int_0^{\infty} p_{\text{in}}(x,0)\, \mathrm{e}^{\mathrm{i}kx} \,\mathrm{d}x \\ &= -\rho_0 A(k) \operatorname{sign}(\operatorname{Re} k)\big(\mathrm{i}k\zeta + \sigma - \operatorname{sign}(\operatorname{Re} k)\omega\big) + 2\mathrm{i}\rho_0 U_0^2 \frac{\mathrm{e}^{-k_0 y_0}}{k - k_0} \\ &= -\mathrm{i}\rho_0 \zeta A(k)|k|K(k) + 2\mathrm{i}\rho_0 U_0^2 \frac{\mathrm{e}^{-k_0 y_0}}{k - k_0} \end{aligned} \tag{15}$$

with Wiener-Hopf kernel

$$K(k) = 1 + \frac{a}{k} - \frac{b}{|k|}, \qquad a = \frac{\sigma}{\mathrm{i}\zeta}, \quad b = \frac{\omega}{\mathrm{i}\zeta}. \tag{16}$$

With $\varepsilon = 0$, $K(k)$ has 0, 1, or 2 zeros in the 1st, 2nd, or 4th quadrant, as shown in table 1, depending on the signs of $\sigma - \omega$ and $\operatorname{Im}\zeta$, and assuming that $\sigma, \omega, \operatorname{Re}\zeta > 0$.

As $K(k)$ has a singularity in $k = 0$, which is inside strip S, we consider the regularised version

$$K(K) = 1 + \frac{a}{k - \mathrm{i}\varepsilon} - \frac{b}{\sqrt{k^2 + \varepsilon^2}}. \tag{17}$$

This $K(k)$ has 3 zeros, which are for small ε approximated as shown in table 2. So in general the zeros and singularities of K are not real and there is a neighbourhood of the real axis where K is analytic.

case	$\sigma-\omega$	$\operatorname{Im}\zeta$	$k_1=-a+b$	$k_2=-a-b$
1	$+$	$+$	$k=k_1\in I$	no solution
2	$+$	$-$	no solution	$k=k_2\in II$
3	$-$	$+$	no solution	no solution
4	$-$	$-$	$k=k_1\in IV$	$k=k_2\in II$

Table 1. Roots of non-regularised WH kernel $K(k)$ in (16)

case	$\sigma-\omega$	$\operatorname{Im}\zeta$	$k_1\simeq -a+b+\mathrm{i}\varepsilon\frac{a}{a-b}$	$k_2\simeq -a-b+\mathrm{i}\varepsilon\frac{a}{a+b}$	$k_3\simeq -\mathrm{i}\varepsilon\frac{a^2+b^2}{a^2-b^2}+\varepsilon^2\frac{8a^3b^2}{(a^2-b^2)^3}$
1	$+$	$+$	$k\simeq -a+b\in I$	no solution	no solution
2	$+$	$-$	no solution	$k\simeq -a-b\in II$	no solution
3	$-$	$+$	no solution	no solution	$k\simeq -\mathrm{i}\varepsilon\frac{a^2+b^2}{a^2-b^2}$
4	$-$	$-$	$k\simeq -a+b\in IV$	$k\simeq -a-b\in II$	$k\simeq -\mathrm{i}\varepsilon\frac{a^2+b^2}{a^2-b^2}$

Table 2. Roots of the regularised WH kernel $K(k)$ in (17)

Hence we arrive at the Wiener-Hopf equation

$$F_-(k)=\rho_0\zeta G_+(k)K(k)+2\mathrm{i}\rho_0U_0^2\frac{\mathrm{e}^{-k_0y_0}}{k-k_0} \tag{18}$$

which is to be solved in the standard way [10] by writing

$$K(k)=\frac{K_+(k)}{K_-(k)} \tag{19}$$

where splitfunction K_+ is analytic in $\mathbb{C}^+$ and K_- is analytic in $\mathbb{C}^-$. These splitfunctions are constructed in the usual way [14] as follows.

Consider $k\in S$ inside a large rectangular contour $\mathcal{C}\subset S$ between $k=-L-\mathrm{i}\eta\varepsilon$ and $k=L+\mathrm{i}\eta\varepsilon$, where η is small enough, as shown in figure 3. In general K has no zeros $k_{1,2,3}$ (if any) within $\mathcal{C}$ and we assume a definition of $\log K(k)$ with branch cuts not crossing S. As it happens, with the present choice of the regularised K, this is achieved by taking the principal value logarithm. Then by Cauchy's integral representation theorem is

$$\log K(k)=\lim_{L\to\infty}\frac{1}{2\pi\mathrm{i}}\int_{\mathcal{C}}\frac{\log K(\xi)}{\xi-k}\,\mathrm{d}\xi=\frac{1}{2\pi\mathrm{i}}\int_{-\infty}^{\infty}\frac{\log K(\xi-\mathrm{i}\eta\varepsilon)}{\xi-\mathrm{i}\eta\varepsilon-k}\,\mathrm{d}\xi-\frac{1}{2\pi\mathrm{i}}\int_{-\infty}^{\infty}\frac{\log K(\xi+\mathrm{i}\eta\varepsilon)}{\xi+\mathrm{i}\eta\varepsilon-k}\,\mathrm{d}\xi \tag{20}$$

where it may be noted that the integrals converge at infinity since

$$\frac{\log K(\xi)}{\xi-k}=O(1/\xi^2)\quad(\xi\to\infty).$$

Considered as a function of k, the first integral can be analytically continued to $\mathbb{C}^+$, and the second

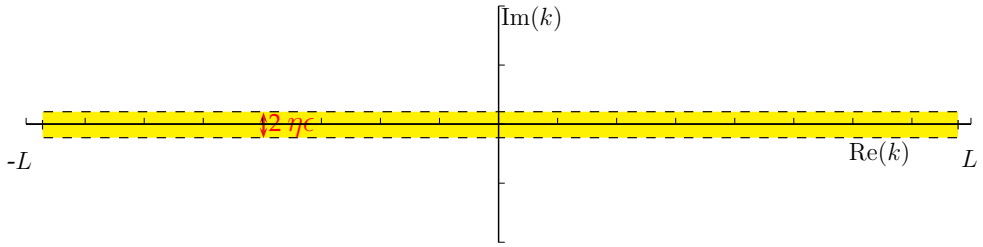

Figure 3. Contour $\mathcal{C}$

integral can be analytically continued to $\mathbb{C}^-$. So we can identify

$$\log K_+(k) = \frac{1}{2\pi \mathrm{i}} \int_{-\infty}^{\infty} \frac{\log K(\xi - \mathrm{i}\eta\varepsilon)}{\xi - \mathrm{i}\eta\varepsilon - k} \,\mathrm{d}\xi, \quad k \in \mathbb{C}^+, \tag{21}$$

$$\log K_-(k) = \frac{1}{2\pi \mathrm{i}} \int_{-\infty}^{\infty} \frac{\log K(\xi + \mathrm{i}\eta\varepsilon)}{\xi + \mathrm{i}\eta\varepsilon - k} \,\mathrm{d}\xi, \quad k \in \mathbb{C}^-. \tag{22}$$

If $\varepsilon \to 0$, the representations of K_+ and K_- become the same, in the sense that it becomes K_+ if $k \in \mathbb{C}^+$ and K_- if $k \in \mathbb{C}^-$.

Although the splitfunctions for $\varepsilon > 0$ are only available numerically, it appears (see Appendix B) that for $\varepsilon = 0$ they can be given analytically exactly, by equation (50), albeit by using the somewhat unusual dilogarithm function. Furthermore, by extensive comparison with the numerical versions for very small but non-zero ε, we could verify that the analytical splitfunctions as defined above are indeed the proper limit for $\varepsilon \to 0$. This remarkable result will be important later for the far field analysis of the physical solution represented by a Fourier integral.

Altogether, we can conclude that in S

$$\begin{aligned} F_-(k)K_-(k) - \rho_0\zeta G_+(k)K_+(k) &= 2\mathrm{i}\rho_0 U_0^2 \frac{\mathrm{e}^{-k_0 y_0}}{k - k_0} K_-(k) \\ &= 2\mathrm{i}\rho_0 U_0^2 \,\mathrm{e}^{-k_0 y_0} \frac{K_-(k) - K_-(k_0)}{k - k_0} + 2\mathrm{i}\rho_0 U_0^2 \frac{\mathrm{e}^{-k_0 y_0}}{k - k_0} K_-(k_0), \end{aligned} \tag{23}$$

where we isolated pole $k_0 \in \mathbb{C}^-$ from K_-. The parts that are analytic in $\mathbb{C}^+$ and in $\mathbb{C}^-$ respectively, are via their equivalence in S each other's analytic continuations, and define an entire function E

$$\begin{aligned} E(k) &= F_-(k)K_-(k) - 2\mathrm{i}\rho_0 U_0^2 \,\mathrm{e}^{-k_0 y_0} \frac{K_-(k) - K_-(k_0)}{k - k_0} \\ &= \rho_0\zeta G_+(k)K_+(k) + 2\mathrm{i}\rho_0 U_0^2 \frac{\mathrm{e}^{-k_0 y_0}}{k - k_0} K_-(k_0). \end{aligned} \tag{24}$$

E can be determined from the condition for $k \to \infty$, related to the edge condition for $(x, y) \to 0$. Following Appendix D, we have $E \equiv 0$, hence we can write from (15) and (24)

$$\begin{aligned} F_-(k) &= 2\mathrm{i}\rho_0 U_0^2 \,\mathrm{e}^{-k_0 y_0} \frac{K_-(k) - K_-(k_0)}{(k - k_0)K_-(k)}, \\ G_+(k) &= \frac{-2\mathrm{i}U_0^2}{\zeta} \frac{\mathrm{e}^{-k_0 y_0}}{k - k_0} \frac{K_-(k_0)}{K_+(k)}, \\ A(k) &= \frac{2U_0^2}{\zeta} \frac{\mathrm{e}^{-k_0 y_0}}{k - k_0} \frac{K_-(k_0)}{|k| K_+(k)}. \end{aligned} \tag{25}$$

$A(k)$ obtained from (25) can be substituted back into (11). This gives, with the inverse Fourier transform from (9) added to the initial field (7), the formal solution u, v and p of the problem.

$$
\begin{aligned}
u &= u_{\text{in}} + \frac{1}{2\pi}\int_{-\infty}^{\infty} \operatorname{sign}(\operatorname{Re} k)\frac{2U_0^2}{\zeta}\frac{\mathrm{e}^{-k_0 y_0}}{k-k_0}\frac{K_-(k_0)}{K_+(k)}\,\mathrm{e}^{-|k|y}\,\mathrm{e}^{-\mathrm{i}kx}\,\mathrm{d}k \\
v &= v_{\text{in}} + \frac{1}{2\pi}\int_{-\infty}^{\infty} -\mathrm{i}\frac{2U_0^2}{\zeta}\frac{\mathrm{e}^{-k_0 y_0}}{k-k_0}\frac{K_-(k_0)}{K_+(k)}\,\mathrm{e}^{-|k|y}\,\mathrm{e}^{-\mathrm{i}kx}\,\mathrm{d}k \\
p &= p_{\text{in}} + \frac{1}{2\pi}\int_{-\infty}^{\infty} \rho_0(\Omega - \operatorname{sign}(\operatorname{Re} k)\sigma)\frac{2U_0^2}{\zeta}\frac{\mathrm{e}^{-k_0 y_0}}{k-k_0}\frac{K_-(k_0)}{|k|K_+(k)}\,\mathrm{e}^{-|k|y}\,\mathrm{e}^{-\mathrm{i}kx}\,\mathrm{d}k.
\end{aligned}
\tag{26}
$$

We notice that the expressions of u and v are integrable at $k = 0$, while the pole $k = k_0$ is included if $x > 0$. Indeed it corresponds to trailing vorticity [8] of the hard-soft discontinuity. The singularity at $k = 0$ is, unlike the one at $k = k_0$, not a pole and has a different origin. Due to this singularity, if not integrable, the Fourier transformation of the pressure in (26) becomes too singular to be interpreted normally and diverges for $r \to \infty$. When we consider the incompressible problem as an inner problem of a larger compressible problem, as in [15, 4, 16, 17], this divergent behaviour disappears as it changes into an outward radiating acoustic wave. The inverse Fourier transform for pressure p is then calculated by splitting off the singular part and interpreting the singular integral in generalised sense [18, 19, 8].

V. Hydrodynamic solution

The solution set u, v and p is the solution of incompressible inner problem of a larger compressible acoustic problem. Although a strict Matched Asymptotic Expansion analysis has not been laid out here in detail, we will refer to it as the inner solution.

In order to evaluate the solutions, in the form of Fourier integrals (26), numerically or asymptotically in the far field, we need to know the behaviour of $K_+(k)$ at $k = 0$. The following asymptotic behaviour of $K_+(k \to 0)$ can be confirmed from C.A and C.B

$$
K_+(k) \simeq c_1 k^{-\frac{1}{2}-\mathrm{i}\delta} \quad \text{for} \quad \sigma < \omega \quad \text{and} \quad K_+(k) \simeq c_1 k^{-\mathrm{i}\delta} \quad \text{for} \quad \sigma > \omega, \tag{27}
$$

where c_1 is a complex constant and $\delta = \frac{1}{2\pi}\log|\frac{\sigma+\omega}{\sigma-\omega}|$ is real positive.

V.A. Solution of velocities u and v

We see by combining (27) and (26) that in either case, the velocities u and v are integrable at $k = 0$. Shown in figure 5 (top and middle) are the solutions (total = incident + scattered) of velocities for a typical representative case. Apparently, the high mean shear intensifies the velocity field especially downstream the edge.

V.B. Solution of pressure p

As we noticed, the behaviour of the singularity at $k = 0$ is different for the cases $\sigma < \omega$ and $\sigma > \omega$. Hence, the far field solution in pressure is different for these cases. This splits our problem into 2 different cases in terms of radiated pressure. We will discuss this in separate sections.

V.B.1. Low shear

The low shear case corresponds with $\sigma < \omega$, *i.e.* $k_0 y_0 > 1$. The behaviour of $K_+ \sim k^{-\frac{1}{2}-\mathrm{i}\delta}$ in the limit $k \to 0$ weakens the non-integrable singularity $|k|^{-1}$ to an integrable singularity $k^{-\frac{1}{2}+\mathrm{i}\delta}$ of the integrand in (26). Hence the pressure solution can be obtained by direct integration like the velocities. For a typical case, this is shown in figure 5 (bottom left). It can be predicted even at this stage that a weaker singularity at $k = 0$ produces a weaker far field sound.

V.B.2. High shear

The high shear case corresponds with $\sigma > \omega$, *i.e.* $k_0 y_0 < 1$. The behaviour of $K^+ \sim k^{-\mathrm{i}\delta}$ in the limit $k \to 0$ does not weaken the singularity in this case and the integral function behaves as $\sim |k|^{-1+\mathrm{i}\delta}$ as $k \to 0$ and hence diverges. The divergent behaviour at $k = 0$ in Fourier space suggests a strong far field at $r = \sqrt{x^2 + y^2} \to \infty$ in the physical plane. The Fourier representation of pressure is too singular to interpret and hence should be regularised, using generalised functions, by splitting off the singular part and the part which is integrable. From (26), we have

$$\begin{aligned}
\overline{p}(x,y) = {} & \frac{\rho_0 U_0^2}{\zeta\pi}\,\mathrm{e}^{-k_0 y_0}\,K_-(k_0)\int_{-\infty}^{0}\left(\frac{\Omega+\sigma}{(k-k_0)|k|K_+(k)} - \frac{\omega+\sigma}{-k_0|k|c_1 k^{-\mathrm{i}\delta}}\right)\mathrm{e}^{-\mathrm{i}kx-|k|y}\,\mathrm{d}k \\
& + \frac{\rho_0 U_0^2}{\zeta\pi}\,\mathrm{e}^{-k_0 y_0}\,K_-(k_0)\int_{0}^{\infty}\left(\frac{\Omega-\sigma}{(k-k_0)|k|K_+(k)} - \frac{\omega-\sigma}{-k_0|k|c_1 k^{-\mathrm{i}\delta}}\right)\mathrm{e}^{-\mathrm{i}kx-|k|y}\,\mathrm{d}k \\
& + \frac{\rho_0 U_0^2}{\zeta\pi}\,\mathrm{e}^{-k_0 y_0}\,\frac{K_-(k_0)}{-c_1 k_0}\left[\int_{-\infty}^{0}\frac{\omega+\sigma}{|k|k^{-\mathrm{i}\delta}}\,\mathrm{e}^{-\mathrm{i}kx-|k|y}\,\mathrm{d}k + \int_{0}^{\infty}\frac{\omega-\sigma}{|k|k^{-\mathrm{i}\delta}}\,\mathrm{e}^{-\mathrm{i}kx-|k|y}\,\mathrm{d}k\right] \qquad (28)
\end{aligned}$$

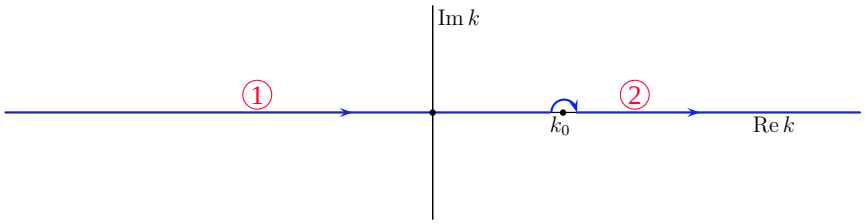

Figure 4. Integration contour

The split of the singularity renders the integrals of $\overline{p}(k,y)$ to be $O(1)$ at $k = 0$ and hence integrable. In (28), the first 2 integrals have a finite limit at $k = 0$ and therefore can be evaluated along the integration contour 1 and 2 respectively, as shown in figure 4. The last integrals in (28) are those which carry the singularity and diverge at $k = 0$ which makes them difficult to interpret. They can be evaluated as generalised functions [18, 19]. With Appendix E, we have

$$\begin{aligned}
& \frac{\rho_0 U_0^2}{\zeta\pi c_1}\,\mathrm{e}^{-k_0 y_0}\,\frac{K_-(k_0)}{-k_0}\left[\int_{-\infty}^{0}\frac{\omega+\sigma}{|k|k^{-\mathrm{i}\delta}}\,\mathrm{e}^{-\mathrm{i}kx-|k|y}\,\mathrm{d}k + \int_{0}^{\infty}\frac{\omega-\sigma}{|k|k^{-\mathrm{i}\delta}}\,\mathrm{e}^{-\mathrm{i}kx-|k|y}\,\mathrm{d}k\right] \\
& \qquad = \frac{\rho_0 U_0^2}{\zeta\pi c_1}\,\mathrm{e}^{-k_0 y_0}\,\frac{K_-(k_0)}{-k_0}\mathrm{i}^{-\mathrm{i}\delta}\Gamma(\mathrm{i}\delta)\left[(\omega+\sigma)z^{-\mathrm{i}\delta} + (\omega-\sigma)\overline{z}^{\,-\mathrm{i}\delta}\right], \qquad (29)
\end{aligned}$$

where $z = x + \mathrm{i}y$. The results from (29) used with the first two integrals in (28) added to the initial field p_{in} gives the final solution of the inner pressure p (50). Shown in figure 5 (bottom right) is the pressure for a typical case. The pressure field is clearly more intense for high than for low shear.

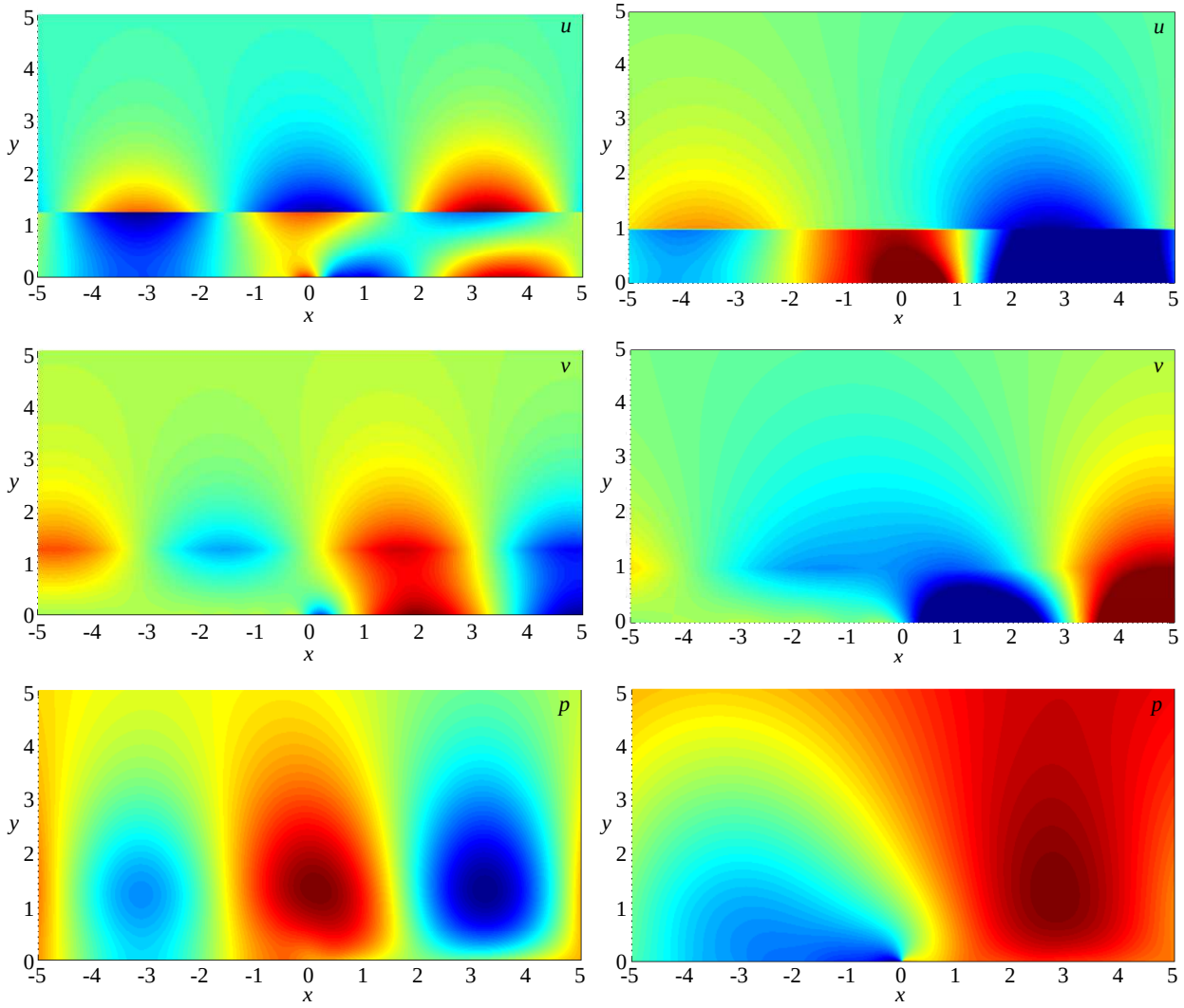

Figure 5. The solution fields u, v and p for low shear $\sigma = 4 < \omega = 5$, $y_0 = 1.25$ (left) and high shear $\sigma = 5 > \omega = 4$, $y_0 = 1$ (right), while $\zeta = \frac{1}{2}(1+\mathrm{i}), U_0 = 5$.

V.C. Far field of inner solution $\overline{p}_{\text{inner}}$ – inside shear layer

In order to have an estimate of the far field radiated pressure, we need the asymptotic evaluation of the pressure integral (26) in the limit $k \to 0$ because small k in Fourier space relates to large $r = \sqrt{x^2+y^2} \sim \infty$ in the physical plane.

(a) Low shear, $\sigma < \omega$:

From (26) and (27), we have in the limit $k \to 0$,

$$\begin{aligned}
\overline{p}(x,y)_{\sigma<\omega} &\sim \overline{p}_{\text{inner }(\sigma<\omega)} \\
&\simeq \frac{\rho_0 U_0^2}{\zeta\pi c_1}\,\mathrm{e}^{-k_0 y_0}\,\frac{K_-(k_0)}{-k_0}\left[(\omega+\sigma)\int_{-\infty}^{0}\frac{\mathrm{e}^{-\mathrm{i}kx-|k|y}}{|k|k^{-\frac{1}{2}-\mathrm{i}\delta}}\,\mathrm{d}k+(\omega-\sigma)\int_{0}^{\infty}\frac{\mathrm{e}^{-\mathrm{i}kx-|k|y}}{|k|k^{-\frac{1}{2}-\mathrm{i}\delta}}\,\mathrm{d}k\right] \\
&= \frac{\rho_0 U_0^2}{\zeta\pi c_1}\,\mathrm{e}^{-k_0 y_0}\,\frac{K_-(k_0)}{-k_0}\left[(-1)^{(\frac{1}{2}+\mathrm{i}\delta)}(\omega+\sigma)\int_{0}^{\infty}\frac{\mathrm{e}^{ikz}}{k^{\frac{1}{2}-\mathrm{i}\delta}}\,\mathrm{d}k+(\omega-\sigma)\int_{0}^{\infty}\frac{\mathrm{e}^{-ik\overline{z}}}{k^{\frac{1}{2}-\mathrm{i}\delta}}\,\mathrm{d}k\right] \qquad (30)
\end{aligned}$$

where $z = x + \mathrm{i}y$. The integrals converge, and can be evaluated like

$$\int_0^\infty \frac{\mathrm{e}^{ikz}}{k^{\frac{1}{2}-\mathrm{i}\delta}}\,\mathrm{d}k = \frac{\Gamma(\frac{1}{2}+\mathrm{i}\delta)}{(-\mathrm{i}z)^{\frac{1}{2}+\mathrm{i}\delta}}. \tag{31}$$

The net innerfield pressure is then given by

$$\overline{p}_{\text{inner}\,(\sigma<\omega)} \simeq \mathrm{i}^{-(\frac{1}{2}+\mathrm{i}\delta)}\Gamma(\tfrac{1}{2}+\mathrm{i}\delta)\frac{\rho_0 U_0^2}{\zeta\pi c_1}\,\mathrm{e}^{-k_0 y_0}\,\frac{K_-(k_0)}{-k_0}\left((\omega+\sigma)z^{-\frac{1}{2}-\mathrm{i}\delta} + (\omega-\sigma)\overline{z}^{-\frac{1}{2}-\mathrm{i}\delta}\right) \tag{32}$$

with $z = r\,\mathrm{e}^{\mathrm{i}\theta}$. The pressure decays as $r^{-\frac{1}{2}}$, which thus limits its effective acoustic source strength.

(b) High shear, $\sigma > \omega$:

The singularity in this case is stronger than the one in the previous case, which enables us to assess that the radiated pressure $\overline{p}_{\text{inner}\,(\sigma>\omega)}$ field must be stronger. The asymptotic behaviour of the integral (26) at $k \to 0$ is essentially the singularity taken out from the integral in (28). Hence the outer limit $r \to \infty$ of the inner pressure field $\overline{p}$ (with $z = r\,\mathrm{e}^{\mathrm{i}\theta}$) is given by (29) as:

$$\overline{p}_{\text{inner}\,(\sigma>\omega)} \simeq \mathrm{i}^{-\mathrm{i}\delta}\Gamma(\mathrm{i}\delta)\frac{\rho_0 U_0^2}{\zeta\pi c_1}\,\mathrm{e}^{-k_0 y_0}\,\frac{K_-(k_0)}{-k_0}\left[(\omega+\sigma)z^{-\mathrm{i}\delta} + (\omega-\sigma)\overline{z}^{-\mathrm{i}\delta}\right]. \tag{33}$$

An important difference is that the modulus of the pressure field varies with r like $|r^{-\mathrm{i}\delta}| = 1$, *i.e.* remains constant rather than decays, and is therefore much stronger than in the previous case. Physically this may be interpreted as mean flow energy being continuously drawn to the hydrodynamic perturbation field and thus contributing to the acoustic energy of the radiated field.

The above far field limit is taken inside the uniform shear flow, which means that we have a diverging mean flow velocity $U = \sigma y \to \infty$ as $y \to \infty$ which is not very physical. Although both (32) and (33) *do* satisfy the prevailing equations, we just want to make sure that no unphysical artefacts are created. So we curtail the shear at height h and define the mean flow being a constant U_∞ beyond $y > h$. This is explained in the next section.

V.D. Far field of inner solution – outside shear layer

In order to approximate the solution outside the shear layer we assume a piecewise smooth transition of the shear layer at $y = h$ where it becomes straight as shown in figure 6, *i.e.*

$$\begin{aligned} U &= \sigma y, \qquad && y < h, \\ U &= U_\infty, \qquad && y \geqslant h. \end{aligned}$$

Let us assume that $h \gg y_0$, so that the source does not interfere with the transition layer. The assumption is based on the physical understanding that the vortical field decays exponentially off the line $y = y_0$. Under this assumption, the incident field p_{in} is negligible near the interface, while the inner pressure field $\overline{p}_{\text{inner}}$ is reflected back as $\overline{p}_{\text{ref}}$ without further interaction with the wall, and transmitted as $\overline{p}_{\text{tra}}$ into the far field. Hence, we may match the outer acoustic field to $\overline{p}_{\text{tra}}$ in order to obtain a more realistic value of the far field sound. In order to obtain $\overline{p}_{\text{tra}}$, we apply the continuity

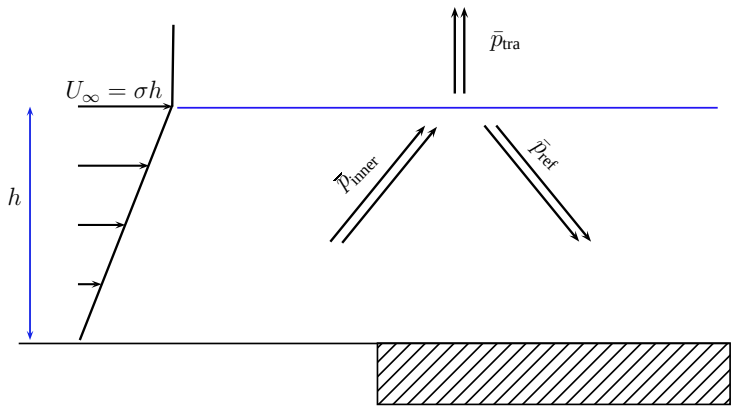

Figure 6. Inner pressure reflected and transmitted at interface $y = h$.

of pressure and velocity at the boundary $y = h$. In the Fourier domain, we have for $y < h$ representation (26), which is for the Fourier transforms

$$\tilde{p}(k,y) = \rho_0 D\big(\Omega_\infty - \operatorname{sign}(\operatorname{Re} k)\sigma\big)\,\mathrm{e}^{-|k|(y-h)}, \quad \tilde{v}(k,y) = -\mathrm{i}D|k|\,\mathrm{e}^{-|k|(y-h)},$$
$$D = \frac{2U_0^2}{\zeta}\frac{\mathrm{e}^{-k_0 y_0}}{k-k_0}\frac{K_-(k_0)}{|k|K_+(k)}\,\mathrm{e}^{-|k|h}, \quad \Omega_\infty = \omega - kU_\infty.$$

The reflected and transmitted variables are given as

$$\tilde{p}_{\text{ref}}(k,y) = \rho_0 R(\Omega_\infty + \operatorname{sign}(\operatorname{Re} k)\sigma)\,\mathrm{e}^{|k|(y-h)}, \qquad \tilde{p}_{\text{tra}}(k,y) = \rho_0 T\Omega_\infty\,\mathrm{e}^{-|k|(y-h)}$$
$$\tilde{v}_{\text{ref}}(k,y) = \mathrm{i}R|k|\,\mathrm{e}^{|k|(y-h)}, \qquad \tilde{v}_{\text{tra}}(k,y) = -\mathrm{i}T|k|\,\mathrm{e}^{-|k|(y-h)}$$

where reflection and transmission coefficients R and T are obtained from the conditions of continuity of pressure and velocity at $y = h$

$$\tilde{p}(k,h) + \tilde{p}_{\text{ref}}(k,h) = \tilde{p}_{\text{tra}}(k,h)$$
$$\tilde{v}(k,h) + \tilde{v}_{\text{ref}}(k,h) = \tilde{v}_{\text{tra}}(k,h).$$

The two linear equations in variables T and R

$$\begin{aligned} \rho_0 D\big(\Omega_\infty - \operatorname{sign}(\operatorname{Re} k)\sigma\big) + \rho_0 R(\Omega_\infty + \operatorname{sign}(\operatorname{Re} k)\sigma) &= \rho_0 T\Omega_\infty, \\ -\mathrm{i}D|k| \qquad\qquad + \quad \mathrm{i}R|k| \qquad\qquad &= -\mathrm{i}T|k|, \end{aligned}$$

can be solved to yield

$$T = D\frac{\Omega_\infty}{\Omega_\infty + \frac{1}{2}\operatorname{sign}(\operatorname{Re} k)\sigma}, \qquad R = D\frac{\frac{1}{2}\operatorname{sign}(\operatorname{Re} k)\sigma}{\Omega_\infty + \frac{1}{2}\operatorname{sign}(\operatorname{Re} k)\sigma}.$$

The inner pressure transmitted outside the shear is then

$$\bar{p}_{\text{tra}}(x,y) = \frac{1}{2\pi}\int_{-\infty}^{\infty}\frac{2\rho_0 U_0^2}{\zeta}\,\frac{\mathrm{e}^{-k_0 y_0}\,K_-(k_0)}{k-k_0}\left[\frac{\Omega_\infty^2}{\Omega_\infty + \frac{1}{2}\operatorname{sign}(\operatorname{Re} k)\sigma}\right]\frac{\mathrm{e}^{-\mathrm{i}kx-|k|y}}{|k|K_+(k)}\,\mathrm{d}k. \tag{34}$$

If we write $\Omega_\infty = \omega - k\sigma h$, the outer limit of the inner pressure can be obtained by the asymptotic evaluation of the integral (34) in the limit $k \to 0$,

$$\bar{p}_{\text{tra}}(x,y) = \frac{\rho_0 U_0^2}{\pi\zeta}\frac{\mathrm{e}^{-k_0 y_0}}{-k_0}K_-(k_0)\left(\int_{-\infty}^{0}\left[\frac{\omega^2}{\omega - \frac{1}{2}\sigma}\right]\frac{\mathrm{e}^{-\mathrm{i}kx-|k|y}}{|k|K_+(k)}\,\mathrm{d}k + \int_0^{\infty}\left[\frac{\omega^2}{\omega + \frac{1}{2}\sigma}\right]\frac{\mathrm{e}^{-\mathrm{i}kx-|k|y}}{|k|K_+(k)}\,\mathrm{d}k\right).$$

In the case of $\sigma < \omega$, using (27) and (31), we obtain

$$\bar{p}_{\text{tra}\,(\sigma<\omega)} = \mathrm{i}^{-(\frac{1}{2}+\mathrm{i}\delta)}\Gamma(\tfrac{1}{2}+\mathrm{i}\delta)\frac{\rho_0 U_0^2}{\zeta\pi c_1}\,\mathrm{e}^{-k_0 y_0}\,\frac{K_-(k_0)}{-k_0}\left[\frac{\omega^2}{\omega-\frac{1}{2}\sigma}z^{-\frac{1}{2}-\mathrm{i}\delta}+\frac{\omega^2}{\omega+\frac{1}{2}\sigma}\overline{z}^{-\frac{1}{2}-\mathrm{i}\delta}\right]. \quad (35)$$

In the other case, *i.e.* $\sigma > \omega$, using (27) and (29), we have

$$\bar{p}_{\text{tra}\,(\sigma>\omega)} = \mathrm{i}^{-\mathrm{i}\delta}\Gamma(\mathrm{i}\delta)\frac{\rho_0 U_0^2}{\zeta\pi c_1}\,\mathrm{e}^{-k_0 y_0}\,\frac{K_-(k_0)}{-k_0}\left[\frac{\omega^2}{\omega-\frac{1}{2}\sigma}z^{-\mathrm{i}\delta}+\frac{\omega^2}{\omega+\frac{1}{2}\sigma}\overline{z}^{-\mathrm{i}\delta}\right]. \quad (36)$$

where $z = r\,\mathrm{e}^{\mathrm{i}\theta}$. We conclude from (32), (33), (35) and (36) that the inclusion of the transition layer does not change the functional relationship of the sound radiated to farfield and differ by only a constant. We will match the outerfield acoustic solution to both inner fields in the next section.

VI. Outer solution and asymptotic matching

Since the mean flow Mach number is small, the inner problem is incompressible. We assume the outer acoustic field, where the mean flow velocity profile changed from linear $U(y) = \sigma y$ to a constant, compressible but with negligible mean flow. Then we have the equation

$$\nabla^2 p + \kappa^2 p = 0, \qquad \kappa = \frac{\omega}{c_0}.$$

With a point source in $x = y = 0$, assuming a certain symmetry in r and θ (where $x = r\cos\theta$ and $y = r\sin\theta$), we search for solutions of the form

$$p(r,\theta) = \gamma(r)\beta(\theta). \quad (37)$$

If we substitute this in the equations we find

$$\gamma'' + \frac{1}{r}\gamma' + \kappa^2\gamma = \frac{\nu^2}{r^2}\gamma, \quad \beta'' + \nu^2\beta = 0,$$

such that

$$\beta(\theta) = B_1\,\mathrm{e}^{\mathrm{i}\nu\theta} + B_2\,\mathrm{e}^{-\mathrm{i}\nu\theta}$$

and

$$\gamma(r) = mH_\nu^{(2)}(\kappa r) + nH_{-\nu}^{(2)}(\kappa r) = mH_\nu^{(2)}(\kappa r) + n\,\mathrm{e}^{-\nu\pi\mathrm{i}}\,H_\nu^{(2)}(\kappa r) = MH_\nu^{(2)}(\kappa r) \quad (38)$$

with the relationship $H_{-\nu}^{(2)}(\kappa r) = \mathrm{e}^{-\mathrm{i}\nu\pi}\,H_\nu^{(2)}(\kappa r)$ [20]. Clearly, M is superfluous but is kept for convenience. The constants B_1, B_2 and ν are to be determined from the matching condition at $r \to 0$ where the Hankel function has the following asymptotic behaviour [20]

$$H_\nu^{(2)}(\kappa r) \simeq \frac{\mathrm{i}}{\pi}\Gamma(\nu)(\tfrac{1}{2}\kappa r)^{-\nu} = \alpha r^{-\nu} \quad (39)$$

with $\mathrm{Re}(\nu) > 0$ and constant $\alpha = \mathrm{i}\pi^{-1}\Gamma(\nu)(\frac{1}{2}\kappa)^{-\nu}$. If ν is purely imaginary, the $r^{-\nu}$-term does not dominate any more for small r and we find [20]

$$H_\nu^{(2)}(\kappa r) \simeq \frac{\mathrm{i}}{\pi}\big(\Gamma(\nu)(\tfrac{1}{2}\kappa r)^{-\nu} + \mathrm{e}^{\mathrm{i}\nu\pi}\,\Gamma(-\nu)(\tfrac{1}{2}\kappa r)^{\nu}\big) = \alpha r^{-\nu} + \tilde{\alpha} r^{\nu}, \quad (40)$$

with $\tilde{\alpha} = \mathrm{i}\pi^{-1}\,\mathrm{e}^{\mathrm{i}\nu\pi}\,\Gamma(-\nu)(\frac{1}{2}\kappa)^{\nu}$. From (37), (38) and (39) or (40), we have for $r \to 0$

$$p(r,\theta) \simeq \alpha r^{-\nu}(B_1\,\mathrm{e}^{\mathrm{i}\nu\theta} + B_2\,\mathrm{e}^{-\mathrm{i}\nu\theta}), \quad \text{resp.} \quad (\alpha r^{-\nu} + \tilde{\alpha} r^{\nu})(B_1\,\mathrm{e}^{\mathrm{i}\nu\theta} + B_2\,\mathrm{e}^{-\mathrm{i}\nu\theta}), \quad (41)$$

to be matched with the outer limit of the inner solutions (32), (33).

VI.A. Farfield sound, low shear case

For low shear, $\sigma < \omega$, the asymptotic matching of (41) with (32) or (35) leads to the following expression of ν and M, given by

$$\nu = \tfrac{1}{2} + \mathrm{i}\delta, \qquad M = \mathrm{i}^{-\frac{3}{2}-\mathrm{i}\delta}\frac{\rho_0 U_0^2}{\zeta c_1}\,\mathrm{e}^{-k_0 y_0}\,\frac{K_-(k_0)}{-k_0}\left(\tfrac{1}{2}\kappa\right)^{\frac{1}{2}+\mathrm{i}\delta}, \tag{42}$$

while B_1 and B_2 represent the different matching with the inner pressure $\overline{p}_{\text{inner }(\sigma<\omega)}$ inside, or $\bar{p}_{\text{tra }(\sigma<\omega)}$ outside the shear layer.

$$\begin{aligned} &B_1 = \omega - \sigma \quad \text{and} \quad B_2 = \omega + \sigma \qquad \text{matched with} \quad \overline{p}_{\text{inner }(\sigma<\omega)} \\ &B_1 = \frac{\omega^2}{\omega + \frac{1}{2}\sigma} \quad \text{and} \quad B_2 = \frac{\omega^2}{\omega - \frac{1}{2}\sigma} \qquad \text{matched with} \quad \bar{p}_{\text{tra }(\sigma<\omega)} \end{aligned} \tag{43}$$

This effect of the reflection at the transition layer is for the type of sound field of rather little concern. Eventually, the farfield sound is given by

$$p(r,\theta) = \mathrm{i}^{-\frac{3}{2}-\mathrm{i}\delta}\frac{\rho_0 U_0^2}{\zeta c_1}\,\mathrm{e}^{-k_0 y_0}\,\frac{K_-(k_0)}{-k_0}(\tfrac{1}{2}\kappa)^{(\frac{1}{2}+\mathrm{i}\delta)}\times H_\nu^{(2)}(\kappa r)\left((\omega+\sigma)\,\mathrm{e}^{-\mathrm{i}(\frac{1}{2}+\mathrm{i}\delta)\theta} + (\omega-\sigma)\,\mathrm{e}^{\mathrm{i}(\frac{1}{2}+\mathrm{i}\delta)\theta}\right) \tag{44}$$

when matched with the inner pressure $\overline{p}_{\text{inner }(\sigma<\omega)}$ inside the shear layer, or

$$p(r,\theta) = \mathrm{i}^{-\frac{3}{2}-\mathrm{i}\delta}\frac{\rho_0 U_0^2}{\zeta c_1}\,\mathrm{e}^{-k_0 y_0}\,\frac{K_-(k_0)}{-k_0}(\tfrac{1}{2}\kappa)^{(\frac{1}{2}+\mathrm{i}\delta)}\times H_\nu^{(2)}(\kappa r)\left(\frac{\omega^2}{\omega-\frac{1}{2}\sigma}\,\mathrm{e}^{-\mathrm{i}(\frac{1}{2}+\mathrm{i}\delta)\theta} + \frac{\omega^2}{\omega+\frac{1}{2}\sigma}\,\mathrm{e}^{\mathrm{i}(\frac{1}{2}+\mathrm{i}\delta)\theta}\right) \tag{45}$$

when matched with the inner pressure $\bar{p}_{\text{tra }(\sigma<\omega)}$ transmitted outside the layer. Shown in figure 7 is the farfield sound obtained by above two different matchings. The difference is very small.

VI.B. Farfield sound, high shear case

The successful matching of the low shear case case cannot (as yet) be continued for the high shear case $\sigma > \omega$. As announced in (41), the inner field that behaves like $r^{-\mathrm{i}\delta}$ has to match with an acoustic field that behaves like $\alpha r^{-\mathrm{i}\delta} + \tilde{\alpha} r^{\mathrm{i}\delta}$, which is apparently not possible. At the time of writing we have no explanation, unfortunately, and we should confine our presentation of the high shear case to the incompressible field only. However, the acoustic results are relevant and too interesting to be ignored entirely. So what we will do is to adopt an *incomplete* matching and give, for the record, the results with the $r^{\mathrm{i}\delta}$-term ignored.

Analogous to the previous case we find in that case

$$\nu = \mathrm{i}\delta, \qquad M = \mathrm{i}^{-1-\mathrm{i}\delta}\frac{\rho_0 U_0^2}{\zeta c_1}\,\mathrm{e}^{-k_0 y_0}\,\frac{K_-(k_0)}{-k_0}\left(\tfrac{1}{2}\kappa\right)^{\mathrm{i}\delta}, \tag{46}$$

with B_1 and B_2 remaining the same as in the previous case (43). Hence, our expression of the farfield sound is given by

$$p(r,\theta) = \mathrm{i}^{-1-\mathrm{i}\delta}\frac{\rho_0 U_0^2}{\zeta c_1}\,\mathrm{e}^{-k_0 y_0}\,\frac{K_-(k_0)}{-k_0}(\tfrac{1}{2}\kappa)^{(\mathrm{i}\delta)} H_\nu^{(2)}(\kappa r)\left((\omega+\sigma)\,\mathrm{e}^{\delta\theta} + (\omega-\sigma)\,\mathrm{e}^{-\delta\theta}\right) \tag{47}$$

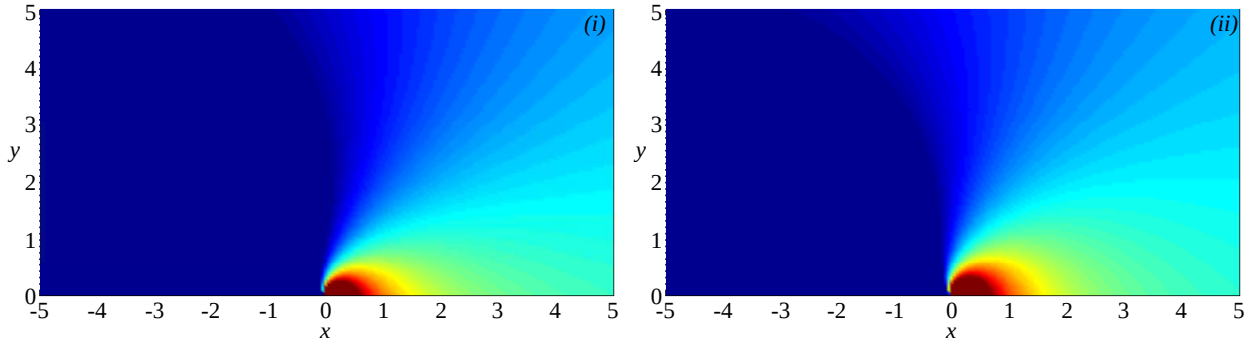

Figure 7. Farfield sound obtained from (44) **and** (45) **respectively.** $\sigma = 4 < \omega = 5, \zeta = \frac{1}{2}(1+\mathrm{i}), U_0 = 5, k_0 = 1, y_0 = 1.25$**.**

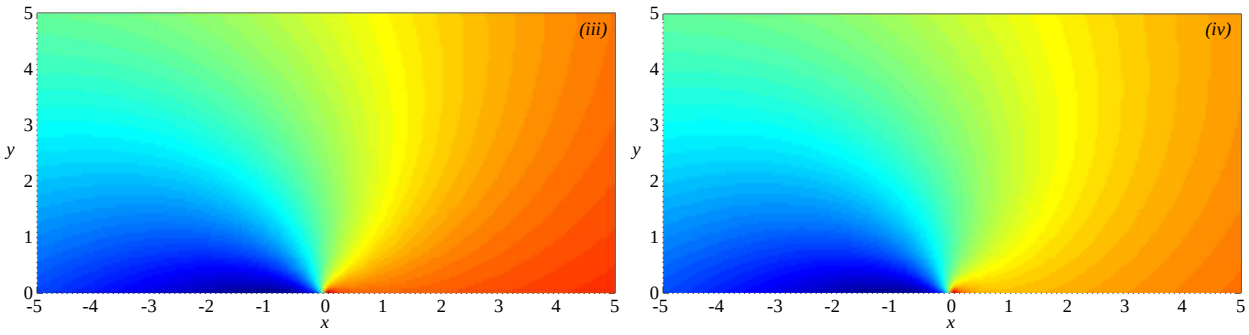

Figure 8. Farfield sound obtained from (*incomplete* matching of) (47) **and** (48) **respectively.** $\sigma = 5 > \omega = 4, \zeta = \frac{1}{2}(1+\mathrm{i}), U_0 = 5, k_0 = 0.8, y_0 = 1$**.**

when matched with the inner pressure $\overline{p}_{\text{inner }(\sigma>\omega)}$, inside the shear layer. Or we have

$$p(r,\theta) = \mathrm{i}^{-1-\mathrm{i}\delta}\frac{\rho_0 U_0^2}{\zeta c_1}\,\mathrm{e}^{-k_0 y_0}\,\frac{K_-(k_0)}{-k_0}\left(\tfrac{1}{2}\kappa\right)^{(\mathrm{i}\delta)} H_\nu^{(2)}(\kappa r)\left(\frac{\omega^2}{\omega-\frac{1}{2}\sigma}\,\mathrm{e}^{\delta\theta}+\frac{\omega^2}{\omega+\frac{1}{2}\sigma}\,\mathrm{e}^{-\delta\theta}\right) \tag{48}$$

when matched with the inner pressure $\overline{p}_{\text{tra }(\sigma>\omega)}$, transmitted outside the layer. Shown in figure 8 (with the above caveat) is the farfield sound obtained by above two different matching.

VII. Conclusions

A systematic and analytically exact solution is obtained by means of the Wiener-Hopf technique of the problem of vorticity, convected by a linearly sheared mean flow, is scattered by the hard-soft transition of the wall. It is illustrated by numerical examples. A particular feature is the fact that the Wiener-Hopf kernel can be split exactly. This enables us to find in rather detail the functional relationship of the hydrodynamic far field and hence the associated acoustic source strength.

The problem appears to be distinguished into two different classes, based upon the relative size of problem parameters σ (the mean flow shear U') and ω (the perturbation frequency), and not (for example) of the impedance of the wall. If the mean shear is relatively weak, *i.e.* if $\sigma < \omega$, the hydrodynamic far field varies as the inverse square root of the distance from the hard-soft singularity. If the mean shear is relatively strong, *i.e.* if $\sigma > \omega$, the hydrodynamic far field tends (in modulus) to a constant.

A way to interpret this non-decaying far field may be the observation that in vortical flow the

energy of perturbations is not conserved [21, 22], and the mean flow may provide the required energy. The present results seems to indicate that for strong enough shear the mean flow is able to provide energy to the perturbations, enough to maintain the strength of the field even away from the hard-soft wall discontinuity.

A problem to be resolved is the incomplete matching of the incompressible inner field with the acoustic outer field for the high shear case, in spite of the fact that the low shear case gives no problems and behaves as expected.

Acknowledgements

We gratefully acknowledge the support from the European Union through ITN-project *FlowAirS* (contract no. FP7-PEOPLE-2011-ITN-289352), with coordinator Yves Aurégan.

We thank Han Slot for his stimulating interest and fruitful discussions.

Appendix

A. Regularising Wiener-Hopf kernel K

The singularity at $k = 0$ of the Wiener-hopf kernel (16)

$$K(k) = 1 + \frac{a}{k} - \frac{b}{\sqrt{k^2}}$$

is regularised by assuming a small $\varepsilon > 0$ with (17)

$$K(k) = 1 + \frac{a}{k - \mathrm{i}\varepsilon} - \frac{b}{\sqrt{k^2 + \varepsilon^2}}$$

with in either case the principal value square root assumed. There is a certain amount of arbitrariness in the way we push the pole at $k = 0$ down (to $k + \mathrm{i}\varepsilon$) or up (to $k - \mathrm{i}\varepsilon$), since the singularity encountered in $\log K(k)$ is a logarithmic one and hence integrable in (21). Whatever we choose, pushing the pole up or downwards, the logarithm has to be defined such that $\log(1) = 0$ and that none of the branch cuts, emanating from the zeros and poles of K, cross the real axis.

case	σ	ω	ζ	$\sigma - \omega$	$\mathrm{Re}(\zeta)$
1	15	2	$1 + \mathrm{i}$	$+$	$+$
2	15	2	$1 - \mathrm{i}$	$+$	$-$
3	4	10	$1 + 10\mathrm{i}$	$-$	$+$
4	4	10	$1 - 10\mathrm{i}$	$-$	$-$

Table 3. 4 cases considered

This is not easy to achieve in general. However, it appears that if we choose for the pole being pushed upwards, $K(k)$ for $k \in \mathbb{R}$ always, *i.e.* for all 4 cases of table 2, avoids the negative real axis (see figure 9), so the standard principal value logarithm is sufficient to take, in which case we have an analytically exact expression (50) for the $\varepsilon = 0$ limit. This is fully confirmed by numerically obtained K_+-integrals for small ε approximating correctly the analytical expression.

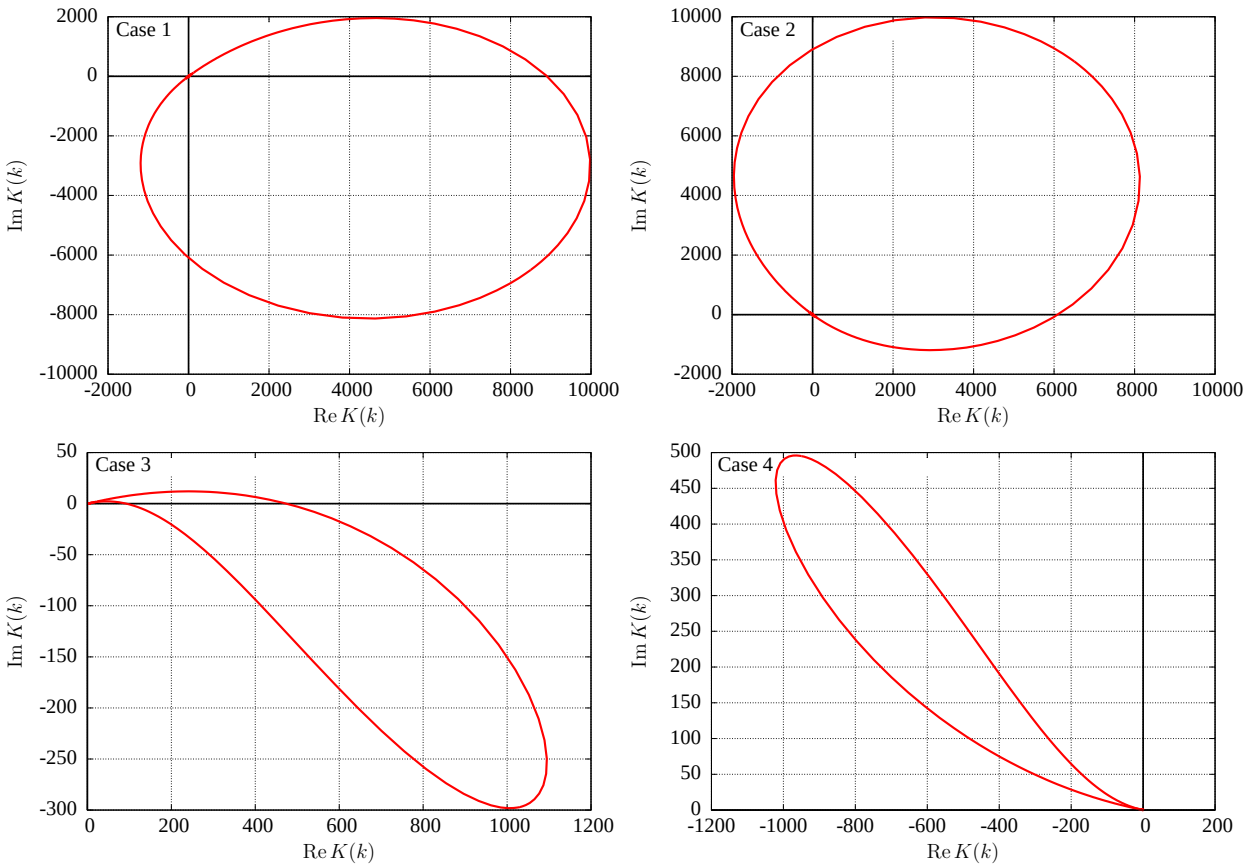

Figure 9. Trace of $K(k)$, $k \in \mathbb{R}$, for all cases of table 3 when the pole at $k = 0$ is regularized with $k = k - \mathrm{i}\varepsilon$. $|k| = \sqrt{k^2 + \varepsilon^2}$, $\varepsilon = 10^{-3}$

It is worth noting that the same happens in case 3 with the pole pushed *down* (*i.e.* with $k + \mathrm{i}\varepsilon$ taken). Also here the trace of K avoids the negative real axis, the principal value log can be taken, and the result approximates the exact expression (50). In conclusion: whenever the principal value log can be taken, there is no difference between the pole being pushed up or downwards.

Consider representative examples of the 4 cases as given in table 3 and graphically displayed in figure 9, where the trace of $K(k)$ is shown for $k \in \mathbb{R}$.

B. Analytical evaluation of the split integral

For $\mathrm{Im}(k) > 0$, the principal value logarithm, and $\varepsilon \to 0$ we have

$$2\pi\mathrm{i} \log K_+(k) = I = \int_{-\infty}^{\infty} \frac{f(x)}{x-k}\,\mathrm{d}x, \quad f(x) = \log\left(1 + \frac{a}{x} - \frac{b}{|x|}\right), \quad a = \frac{\sigma}{\mathrm{i}\zeta},\ b = \frac{\omega}{\mathrm{i}\zeta}.$$

We distinguish

$$\int_{-\infty}^{\infty} \frac{\log(1 + a/x - b/|x|)}{x-k}\,\mathrm{d}x = \int_0^{\infty} \frac{\log(1 + (a-b)/x)}{x-k}\,\mathrm{d}x - \int_0^{\infty} \frac{\log(1 - (a+b)/x)}{x+k}\,\mathrm{d}x,$$

here referred to as I_1 and I_2 respectively. Consider the first integral

$$I_1 = \int_0^{\infty} \frac{\log(1 + q/x)}{x-k}\,\mathrm{d}x$$

where $k, q \in \mathbb{C}$. We transform $x \to 1/x$ and then $qx = y$, to have

$$I_1 = \int_0^\infty \frac{\log(1+qx)}{x(1-kx)}\,\mathrm{d}x = \int_0^{q\cdot\infty} \frac{\log(1+y)}{y(1-ky/q)}\,\mathrm{d}y = \int_0^{q\cdot\infty} \log(1+y)\left(\frac{1}{y} - \frac{1}{y-q/k}\right)\,\mathrm{d}y$$

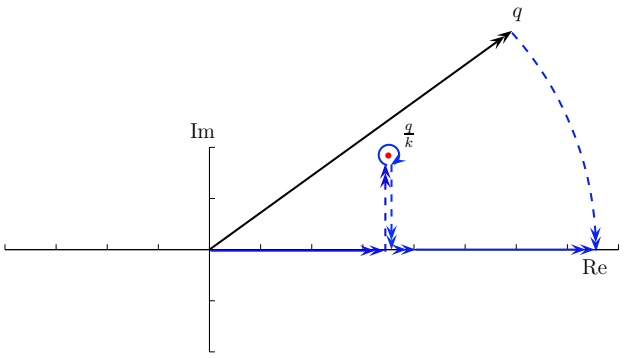

Figure 10. Closure of the integral contour

We close the contour (figure 10) from $y = q \cdot \infty$ to the real axis at $y = \infty$. Denote $\alpha = q/k$ and $\beta = 1 + q/k$. By

$$\begin{aligned} C(k,q) &= -1 \quad \text{if} \qquad 0 < \arg(q/k) < \arg q, \\ C(k,q) &= 1 \quad \text{if} \qquad \arg q < \arg(q/k) < 0, \\ C(k,q) &= 0 \quad \text{otherwise} \end{aligned}$$

we indicate the captured pole in $y = \alpha$. In particular for k is real in the limit from $\mathbb{C}^+$:

$$\begin{aligned} k \in (0,\infty) \;\&\; \operatorname{Im} q > 0 \quad &\Rightarrow \quad C = -1, \\ k \in (-\infty,0) \;\vee\; \operatorname{Im} q < 0 \quad &\Rightarrow \quad C = 0. \end{aligned}$$

We thus find

$$I_1 = \int_0^\infty \log(1+y)\left(\frac{1}{y} + \frac{1}{\alpha - y}\right)\,\mathrm{d}y - 2\pi\mathrm{i}C(k,q)\log\beta.$$

With the use of the following definition of the dilogarithm [20] (with a branch cut along the negative real axis), related to the polylogarithm of order 2,

$$\operatorname{dilog}(z) = \int_1^z \frac{\log t}{1-t}\,\mathrm{d}t = \operatorname{Li}_2(1-z),$$

we write our integral as a limit

$$I_1 = \lim_{N\to\infty} \int_0^N \log(1+y)\left(\frac{1}{y} + \frac{1}{\alpha - y}\right)\,\mathrm{d}y = \lim_{N\to\infty} \int_0^N \frac{\log(1+y)}{y}\,\mathrm{d}y + \lim_{N\to\infty} \int_0^N \frac{\log(1+y)}{\alpha - y}\,\mathrm{d}y. \tag{49}$$

The first integral in (49) is therefore

$$\int_0^N \frac{\log(1+y)}{y}\,\mathrm{d}y = -\int_1^{N+1} \frac{\log z}{1-z}\,\mathrm{d}z = -\operatorname{dilog}(N+1).$$

The second integral is

$$\int_0^N \frac{\log(1+y)}{\alpha-y}\,\mathrm{d}y = \int_1^{N+1} \frac{\log z}{\beta-z}\,\mathrm{d}z = \int_{\beta^{-1}}^{(N+1)\beta^{-1}} \frac{\log t + \log\beta}{1-t}\,\mathrm{d}t =$$
$$\mathrm{dilog}((N+1)\beta^{-1}) - \mathrm{dilog}(\beta^{-1}) - \log\beta\log((N+1)\beta^{-1}-1) + \log\beta\log(\beta^{-1}-1).$$

Altogether, and using the asymptotic behaviour $\mathrm{dilog}(z) \sim -\frac{1}{2}(\log z)^2 + \ldots$ for $z \to \infty$, we have

$$I_1 = \int_0^\infty \frac{\log(1+q/x)}{x-k}\,\mathrm{d}x = \lim_{N\to\infty}\Big[-\mathrm{dilog}(N+1) + \mathrm{dilog}((N+1)\beta^{-1}) - \mathrm{dilog}(\beta^{-1})$$
$$- \log\beta\log((N+1)\beta^{-1}-1) + \log\beta\log(\beta^{-1}-1)\Big] - 2\pi\mathrm{i}C(k,q)\log\beta =$$
$$- \mathrm{dilog}(\beta^{-1}) + \tfrac{1}{2}\log^2(\beta) + \log\beta\log(\beta^{-1}-1) - 2\pi\mathrm{i}C(k,q)\log\beta$$

The second integral I_2 can be performed in the same fashion to obtain the overall expression of $\log K_+$ for $k \in \mathbb{C}^+$ and $\varepsilon \to 0$ as

$$2\pi\mathrm{i}\log K_+(k) = I = -\mathrm{dilog}\Big(\frac{k}{k+a-b}\Big) + \mathrm{dilog}\Big(\frac{k}{k+a+b}\Big)$$
$$+ \tfrac{1}{2}\log^2\Big(\frac{k+a-b}{k}\Big) - \tfrac{1}{2}\log^2\Big(\frac{k+a+b}{k}\Big)$$
$$+ \log\Big(\frac{k+a-b}{k}\Big)\log\Big(\frac{b-a}{k+a-b}\Big) - \log\Big(\frac{k+a+b}{k}\Big)\log\Big(\frac{-b-a}{k+a+b}\Big)$$
$$- 2\pi\mathrm{i}C_1\log\Big(\frac{k+a-b}{k}\Big) + 2\pi\mathrm{i}C_2\log\Big(\frac{k+a+b}{k}\Big), \quad (50)$$

where $C_1 = C(k, a-b)$ and $C_2 = C(-k, -a-b)$. If required, $\log K_-(k)$ with $k \in \mathbb{C}^-$ is similar.

C. Asymptotic analysis of the split integral I for k near 0

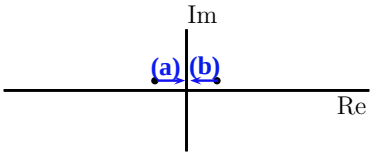

Figure 11. Path of $k \uparrow 0$ and $k \downarrow 0$, with $\mathrm{Im}\,k = +0$.

The behaviour for $k \to 0$ of the integral $I(k)$ and hence $K_+(k)$ is distinct for high shear ($\sigma > \omega$) or low shear ($\sigma < \omega$). In particular, we will show that $K_+ \sim k^{-\mathrm{i}\delta}$ and $K_+ \sim k^{-\frac{1}{2}-\mathrm{i}\delta}$, respectively. Hence we break this analysis into 2 parts. Also, we will assume the natural condition $\mathrm{Re}(\zeta) > 0$. The limit $k \to 0$ is taken from below and from above, along but just above the real axis, as shown in figure 11. In all cases we use the fact that [20]

$$\mathrm{dilog}(z) = \tfrac{1}{6}\pi^2 + O(z\log z) \quad \text{for} \quad z \to 0,$$

making in general the dilog-parts unimportant to leading orders.

C.A. High shear case

This analysis for $k \to 0$ and $\mathrm{Im}\, k = +0$ relates to the high shear ($\sigma > \omega$) cases 1 and 2 in table 2. There is no contribution of the pole q/k, whether we approach from left or right, hence $C_1 = C_2 = 0$.

Case (a): $k \uparrow 0$

With the principal value logarithm and $k \uparrow 0$, we have

$$\log\Big(\frac{k+a+b}{k}\Big) \simeq \log(a+b) - \log(k) + 2\pi\mathrm{i}, \quad \log\Big(\frac{-b-a}{k+a+b}\Big) \simeq -\pi\mathrm{i}.$$
$$\log\Big(\frac{k+a-b}{k}\Big) \simeq \log(a-b) - \log(k) + 2\pi\mathrm{i}, \quad \log\Big(\frac{b-a}{k+a-b}\Big) \simeq -\pi\mathrm{i}.$$

From (50) we have then

$$I \sim \log(k)\log\Big|\frac{a+b}{a-b}\Big| + \tfrac{1}{2}\log^2(a-b) - \tfrac{1}{2}\log^2(a+b) + \pi\mathrm{i}\log\Big(\frac{a-b}{a+b}\Big).$$

Case (b): $k \downarrow 0$

For $k \downarrow 0$, we have

$$\log\Big(\frac{k+a+b}{k}\Big) \simeq \log(a+b) - \log(k), \quad \log\Big(\frac{-b-a}{k+a+b}\Big) \simeq \pi\mathrm{i},$$
$$\log\Big(\frac{k+a-b}{k}\Big) \simeq \log(a-b) - \log(k), \quad \log\Big(\frac{b-a}{k+a-b}\Big) \simeq \pi\mathrm{i}.$$

From 50, we have

$$I \sim \log(k)\log\Big|\frac{a+b}{a-b}\Big| + \tfrac{1}{2}\log^2(a-b) - \tfrac{1}{2}\log^2(a+b) + \pi\mathrm{i}\log\Big(\frac{a-b}{a+b}\Big).$$

We see that the limits from left and right come down to the same expression. As a result, the asymptotic behaviour of K_+ becomes

$$K_+ \sim c_1 k^{-\mathrm{i}\delta}, \quad \delta = \frac{1}{2\pi}\log\Big|\frac{\sigma+\omega}{\sigma-\omega}\Big|, \tag{51}$$

where δ is real positive and c_1 is a complex constant given by

$$c_1 = \mathrm{e}^{\frac{1}{2\pi\mathrm{i}}\left[\frac{1}{2}\log^2(a-b) - \frac{1}{2}\log^2(a+b) + \pi\mathrm{i}\log\left(\frac{a-b}{a+b}\right)\right]} \tag{52}$$

For illustration, figure 12 shows a comparison of a numerically, analytically and asymptotically obtained I.

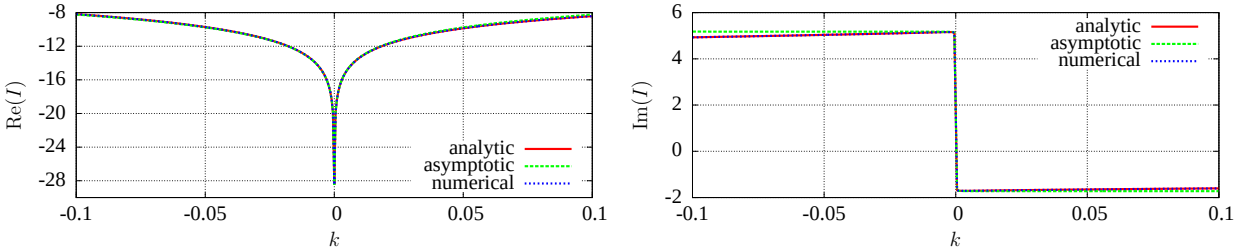

Figure 12. Comparison of the I calculated from analytical, asymptotic and numerical methods for $\sigma = 5 > \omega = 4$ and $\zeta = \frac{1}{2}(1+\mathrm{i})$.

C.B. Low shear case

The asymptotic analysis of (50) for $k \to 0$ and $\mathrm{Im}(k) = +0$ considers the low shear ($\sigma < \omega$) cases 3 and 4 of table 2. Here, we have a contribution of the q/k-pole when we approach from the right.

Case (a): $k \uparrow 0$

With the principal value logarithm and $k \uparrow 0$, the following hold:

$$\log\Big(\frac{k+a+b}{k}\Big) \simeq \log(a+b) - \log(k) + 2\pi\mathrm{i}, \quad \log\Big(\frac{-b-a}{k+a+b}\Big) \simeq -\pi\mathrm{i},$$
$$\log\Big(\frac{k+a-b}{k}\Big) \simeq \log(a-b) - \log(k), \quad \log\Big(\frac{b-a}{k+a-b}\Big) \simeq \pi\mathrm{i}.$$

From (50), we have with $C_1 = C_2 = 0$

$$I \sim \log(k)\left[\log\Big|\frac{a+b}{a-b}\Big| - \pi\mathrm{i}\right] + \tfrac{1}{2}\log^2(a-b) - \tfrac{1}{2}\log^2(a+b) + \pi\mathrm{i}\log\Big(\frac{a-b}{a+b}\Big).$$

Case (b): $k \downarrow 0$

We have

$$\log\Big(\frac{k+a+b}{k}\Big) \simeq \log(a+b) - \log(k), \quad \log\Big(\frac{-b-a}{k+a+b}\Big) \simeq \pi\mathrm{i},$$
$$\log\Big(\frac{k+a-b}{k}\Big) \simeq \log(a-b) - \log(k), \quad \log\Big(\frac{b-a}{k+a-b}\Big) \simeq -\pi\mathrm{i}.$$

Because of the q/k-pole contribution we have $C_1 = -1$ and $C_2 = 0$. From (50), we have

$$I \sim \log(k)\Big[\log\Big|\frac{a+b}{a-b}\Big| - \pi\mathrm{i}\Big] + \tfrac{1}{2}\left(\log^2(a-b) - \log^2(a+b)\right) + \pi\mathrm{i}\log\Big(\frac{a-b}{a+b}\Big).$$

We see that the limiting behaviours from the left and from the right are the same. The asymptotic expression for K_+ is then

$$K_+ \sim c_1 k^{-\frac{1}{2}-\mathrm{i}\delta}, \quad \delta = \frac{1}{2\pi}\log\Big|\frac{\sigma+\omega}{\sigma-\omega}\Big|. \tag{53}$$

where (the same as before) δ is real positive and c_1 is a complex constant given by

$$c_1 = \mathrm{e}^{\frac{1}{2\pi\mathrm{i}}\left[\frac{1}{2}\left(\log^2(a-b)-\log^2(a+b)\right)+\pi\mathrm{i}\log\left(\frac{a-b}{a+b}\right)\right]} \tag{54}$$

For illustration, figure 13 shows a comparison between numerically, analytically and asymptotically obtained I.

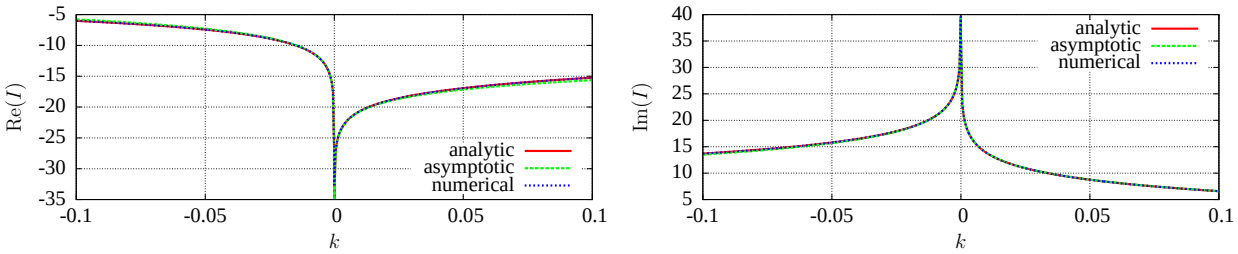

Figure 13. Comparison of I calculated numerically, analytically, and asymptotically for $\sigma = 4 < \omega = 5$ and $\zeta = \frac{1}{2}(1+\mathrm{i})$.

C.C. Asymptotic analysis for k large

The analysis for $k \to \infty$ is useful to derive the edge condition in the next section. Again, we consider $\mathrm{Im}(k) = +0$. Noting that for $z \to 0$ we have $\mathrm{dilog}(1-z) \simeq z + O(z^2)$ and $\log(1+z) = z + O(z^2)$, we may obtain for $k \to \infty$

$$I \simeq \frac{2b}{k}\log k + \frac{a-b}{k}\big(\log(b-a) - 2\pi\mathrm{i}C_1\big) - \frac{a+b}{k}\big(\log(-b-a) - 2\pi\mathrm{i}C_2\big).$$

Overall, the dominating term is $\frac{2b}{k}\log k$.

D. Evaluation of entire function E

E can be determined from the condition at infinity. In order to obtain $E(k)$ for $k \to \infty$, we need the asymptotic behaviour of K_+, $k \to \infty$. From C.C, we have

$$\lim_{k\to\infty} \log K_+(k) = \lim_{k\to\infty} \frac{2b}{2\pi\mathrm{i}k}\log k = 0 \tag{55}$$

so $K_+(k) \to 1$.

The asymptotic behaviour of $G_+(k)$ in the limit $k \to \infty$ is found from the so-called edge condition for $r \to 0$ where r is the distance from the edge. Consider a pressure distribution p at a small distance r from the discontinuity at $r = 0$, such that p is dominated by some power of r, say $p = O(r^\alpha)$. From the momentum equation it follows that the (radial) velocity, say w, should be $w = O(r^{\alpha-1})$. The outward energy flux $\Phi(r)$ across a small circular arc, centred at the edge at

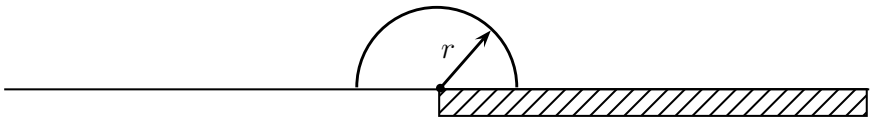

Figure 14. Energy flux across a small semi-circle of radius r around the singularity.

radius r (see figure 14) is then given by

$$\Phi(r) \sim \int_0^\pi pwr\,\mathrm{d}\theta \sim \pi r^\alpha r^{\alpha-1} r \sim r^{2\alpha}. \tag{56}$$

In the absence of a physical source at $r = 0$, the energy flux should vanish for $r \downarrow 0$. Hence we must have $\alpha > 0$.

The function $G_+(k)$ from (13) is therefore

$$G_+(k \to \infty) \sim \int_0^\infty x^{\alpha-1}\,\mathrm{e}^{\mathrm{i}kx}\,\mathrm{d}x = k^{-\alpha}\Gamma(\alpha)\,\mathrm{e}^{\frac{1}{2}\pi\mathrm{i}\alpha} \tag{57}$$

From (24), (55) and (57), we have

$$E(k) = \rho_0\zeta G_+(k)K_+(k) + O(1/k) \sim k^{-\alpha}\cdot 1 \to 0 \quad (k \to \infty). \tag{58}$$

Thus the function $E(k)$ vanishes at $k \to \infty$ and since it is an entire function, it should vanish everywhere, *i.e.* $E(k) = 0$.

E. Regularisation of the diverging integral

We want to assign a meaning to

$$\psi(x,y) = \int_0^\infty \frac{1}{k^{1-\mathrm{i}\delta}}\,\mathrm{e}^{\mathrm{i}kz}\,\mathrm{d}k$$

where $z = x + \mathrm{i}y$ with $y > 0$ and δ is real and nonzero. The integral converges for $k \to \infty$ but not for $k = 0$. Following Lighthill-Jones [18, 19], we define the function $H(k)k^{-1+\mathrm{i}\delta}$ as the generalised derivative

$$\frac{H(k)}{k^{1-\mathrm{i}\delta}} \stackrel{\text{def}}{=} \frac{\mathrm{d}}{\mathrm{d}k}\left(\frac{H(k)}{\mathrm{i}\delta k^{-\mathrm{i}\delta}}\right)$$

and the integral

$$\psi(x,y) = \int_{-\infty}^\infty \frac{\mathrm{d}}{\mathrm{d}k}\left(\frac{H(k)}{\mathrm{i}\delta k^{-\mathrm{i}\delta}}\right)\mathrm{e}^{\mathrm{i}kz}\,\mathrm{d}k = -\int_{-\infty}^\infty \frac{zH(k)}{\delta k^{-\mathrm{i}\delta}}\,\mathrm{e}^{\mathrm{i}kz}\,\mathrm{d}k =$$
$$-z\delta^{-1}\int_0^\infty k^{\mathrm{i}\delta}\,\mathrm{e}^{\mathrm{i}kz}\,\mathrm{d}k = -\mathrm{i}\delta^{-1}\Gamma(1+\mathrm{i}\delta)(-\mathrm{i}z)^{-\mathrm{i}\delta} = \Gamma(\mathrm{i}\delta)(-\mathrm{i}z)^{-\mathrm{i}\delta}.$$

This result is unique and independent of scaling.

References

[1]J. E. Ffowcs Williams, "Sound Radiation from Turbulent Boundary Layers formed on Compliant Surfaces," *Journal of Fluid Mechanics*, Vol. 22, No. 2, 1965, pp. 347–358.

[2]D. G. Crighton, "Radiation from Turbulence near a Composite Flexible Boundary," *Proceedings of the Royal Society of London. A. Mathematical and Physical Sciences*, Vol. 314, No. 1517, 1970, pp. 153–173.

[3]D. G. Crighton, "Radiation from Vortex Filament Motion near a Half Plane," *Journal of Fluid Mechanics*, Vol. 54, 1972, pp. 357–362.

[4]D. G. Crighton, A. P. Dowling, J. E. Ffowcs Williams, M. Heckl, and F. G. Leppington, *Modern Methods in Analytical Acoustics: Lecture Notes*, Springer, 1992.

[5]Y. Aurégan and M. Leroux, "Experimental Evidence of an Instability over an Impedance Wall in a Duct with Flow," *Journal of Sound and Vibration*, Vol. 317, No. 3-5, 2008, pp. 432–439.

[6]Y. Aurégan and D. Marx, "Comparison of Experiments with Stability Analysis Predictions in a Lined Flow Duct," *16th AIAA/CEAS Aeroacoustics Conference*, 2010, AIAA Paper 2010-3946.

[7]A. Powell, "Aerodynamic Noise and the Plane Boundary," *The Journal of the Acoustical Society of America*, Vol. 32, No. 8, 1960, pp. 982–990.

[8]S. W. Rienstra, M. Darau, and E. J. Brambley, "The Trailing Vorticity Field behind a Line Source in Two-dimensional Incompressible Linear Shear Flow," *Journal of Fluid Mechanics*, Vol. 720, 2013, pp. 618–636.

[9]E. J. Brambley, M. Darau, and S. W. Rienstra, "The Critical Layer in Linear-shear Boundary Layers over Acoustic Linings," *Journal of Fluid Mechanics*, Vol. 710, 2012, pp. 545–568.

[10]B. Noble, *Methods Based on the Wiener-Hopf Technique*, Chelsea, 1958.

[11]Lord Rayleigh, *Theory of Sound: Volume 2*, Dover, 1945.

[12]P. G. Drazin and W. H. Reid, *Hydrodynamic Stability*, Cambridge University Press, 2004.

[13]S. A. Orszag and S. C. Crow, "Instability of a Vortex Sheet Leaving a Semi-infinite Plate," *Studies in Applied Mathematics*, Vol. 49, No. 2, 1970, pp. 167–181.

[14]N. Wiener and E. Hopf, "Über eine Klasse singuläre Integralgleichungen," *S.B. Preuss. Akad. Wiss.*, 1931, pp. 696–706.

[15]M. B. Lesser and D. G. Crighton, "Physical Acoustics and the Method of Matched Asymptotic Expansions," *Physical Acoustics Principles and Methods*, edited by W.P. Mason and R.N. Thurston, Vol. 11 of *Physical Acoustics*, Academic Press, 1975, pp. 69–149.

[16]Xuesong Wu, "Generation of Sound and Instability Waves due to Unsteady Suction and Injection," *Journal of Fluid Mechanics*, Vol. 453, 2002, pp. 289–313.

[17]S. W. Rienstra and A. Hirschberg, *An Introduction to Acoustics*, Technische Universiteit Eindhoven, 2012, revised and updated version of IWDE 92-06, `http://www.win.tue.nl/~sjoerdr/papers/boek.pdf`.

[18]D. S. Jones, *The Theory of Generalised Functions*, Cambridge University Press, 1982.

[19]M. J. Lighthill, *Introduction to Fourier Analysis and Generalised Functions*, Cambridge University Press, 1958.

[20]Frank W. J. Olver, Daniel W. Lozier, Ronald F. Boisvert, and Charles W. Clark, *NIST Handbook of Mathematical Functions*, National Institute of Standards and Technology, and Cambridge University Press, 2010.

[21]M. K. Myers, "An Exact Energy Corollary for Homentropic Flow," *Journal of Sound and Vibration*, Vol. 109, 1986, pp. 277–284.

[22]S. W. Rienstra, "Sound Diffraction at a Trailing Edge," *Journal of Fluid Mechanics*, Vol. 108, 1981, pp. 443–460.

PREVIOUS PUBLICATIONS IN THIS SERIES:

Number	Author(s)	Title	Month
14-13	J.C. van der Meer F. Crespo S. Ferrer	Generalized Hopf fibration and geometric SO(3) reduction of the 4DOF harmonic oscillator	Apr. '14
14-14	J. de Graaf	Matrix Gauge fields and Noether's theorem	May '14
14-15	S.P. Korzilius A.C.H. Kruisbrink W.H.A. Schilders M.J.H. Anthonissen T. Yue	Momentum conserving methods that reduce particle clustering in SPH	May '14
14-16	A.S. Tijsseling Q. Hou Z. Bozkus	An improved 1D model for liquid slugs travelling in pipelines	May '14
14-17	S.W. Rienstra D.K. Singh	Hard wall – soft wall – vorticity scattering in shear slow	May '14

Ontwerp: de Tantes,
Tobias Baanders, CWI